Eur. Phys. J. B **35**, 295–300 (2003)
DOI: 10.1140/epjb/e2003-00280-6

THE EUROPEAN PHYSICAL JOURNAL B

Nonlinear properties of ferromagnetic $La_{1-x}Ca_xMnO_3$ single crystals

V. Markovich[1], Y. Yuzhelevski[1], G. Gorodetsky[1], G. Jung[2,a], C.J. van der Beek[2], and Ya.M. Mukovskii[3]

[1] Department of Physics, Ben Gurion University of the Negev, PO Box 653, 84105 Beer Sheva, Israel
[2] Laboratoire des Solides Irradiés, École Polytechnique, 91128 Palaiseau, France
[3] Moscow State Steel and Alloys Institute, 119049 Moscow, Russia

Received 12 May 2003
Published online 15 October 2003 –

Abstract. The resistive and magnetic properties of $La_{1-x}Ca_xMnO_3$ single crystals are investigated. In particular, properties of close-to-critically doped crystals with $x = 0.22$ are confronted with those of underdoped crystals with $x = 0.18$ and $x = 0.2$ and optimally doped crystals with $x = 0.3$. A systematic investigation of nonlinear transport shows that the critically doped crystal does not simply constitute an intermediate case between strongly nonlinear underdoped and linear, optimally doped one. The observed low-temperature resistivity increase can be interpreted in terms of orbital ordering or as a manifestation of an intrinsic tunnelling mechanism. The transport measurements have been completed by magneto-optic investigations which suggest that the low temperature resistivity of the underdoped $x = 0.18$ compound is dominated by tunnelling through intrinsic barriers associated with twin domains, while phase separation dominates in the critically doped $x = 0.22$ compound.

PACS. 75.47.Gk Colossal magnetoresistance – 75.47.Lx Manganites – 71.30.+h Metal-insulator transitions and other electronic transitions

1 Introduction

The nature of charge transport in colossal magnetoresistance (CMR) manganites remains an open question despite a significant effort devoted to that subject. Recently, a lot of attention has been focused on spin dependent transport resulting from a complex interplay between spins of charge carriers and localized magnetic moments [1]. Many experiments show results astonishingly similar to the effects of spin-dependent tunnelling and current induced reversal of magnetization in magnetic tunnel structures [2–4]. The applicability of the spin-tunnelling mechanism is justified by almost 100% spin polarization of charge carriers in CMR manganites [1]. The spin-dependent transport phenomena in bulk CMR samples are, nevertheless, more complex than those seen in thin film magnetic tunnel junctions and artificial multilayer structures. This remains true even for manganite single crystals where spurious effects associated with grain boundaries have been eliminated [5,6].

A growing number of publications relates the basic CMR features of manganites to phase separation. In this respect, low doped $La_{1-x}Ca_xMnO_3$ (LCMO) systems are of a particular interest. The critical doping level $x_C = 0.22$ separates different electronic and magnetic phases in the LCMO phase diagram [7,8]. Above x_C, the LCMO ground state is ferromagnetic and metallic, while samples doped below the critical level have charge/orbital ordered ferromagnetic insulating ground state [8–10]. Moreover, there are strong indications that in the doping range $0.17 < x < 0.25$ there exist a mixed ferromagnetic state composed of insulating and metallic ferromagnetic phases with a different level of orbital ordering (OO) at temperatures below the Curie temperature T_C [11,12].

The transport properties of low-doped LCMO ($x < 0.3$) are extremely sensitive to the doping level x, in particular at very low temperatures [7]. Less-than-critically doped $La_{0.82}Ca_{0.18}MnO_3$ is characterized by strongly nonlinear current-voltage $I - V$ characteristics and the presence of metastable resistivity states [6]. The metastable resistivity is accompanied by the appearance of reproducible structures in the differential conductivity *vs.* voltage characteristics [6,13–15]. The experimental $I - V$ curves of $x = 0.18$ LCMO have been satisfactory described by a model incorporating hopping, metallic, and tunnel

[a] *Present address:* Ben Gurion University of the Negev, also with Instytut Fizyki PAN, Warszawa, Poland
e-mail: jung@bgumail.bgu.ac.il

conductivity channels [6]. The metastable resistivity has been interpreted in terms of spin polarized tunnelling which influences the conditions of phase separation along the current path [6]. The pronounced conductivity oscillations and reproducible structures in $dV/dI(V)$ characteristics were attributed to intrinsic tunnel junctions associated with magnetic domain walls pinned to structural defects [6,13,14]. Random features in the $I-V$ characteristics were found to originate from strongly non-Gaussian fluctuations of the resistivity taking the form of bias-dependent random telegraph noise [13,15].

Optimally doped LCMO, $x = 0.3$, has a pronouncedly metallic, ferromagnetic ground state. One would therefore expect, that the critically doped LCMO should constitute an intermediate case between strongly nonlinear underdoped and linear quasi-metallic optimally doped system. In this paper we report on the transport and magnetic properties of very close-to-critically doped $La_{0.78}Ca_{0.22}MnO_3$, and confront them with those of underdoped $x = 0.18$ and optimally doped $x = 0.3$ LCMO systems. The experiments reveal that not all of the properties of the critically doped LCMO follow the "intermediate case" scenario. Magneto-optical investigations show that the influence of tunnel conduction on the nonlinear conductivity of the LCMO system is controlled not only by the doping level but also by the micro-crystalline properties of the sample and the degree of twinning.

2 Experimental

The LCMO crystals were grown by a floating zone method using radiative heating [16]. The crystals grow in a cylindrical shape, 3–5 mm in diameter and 35–40 mm long with the axis close to $\langle 110 \rangle$ crystalline direction. The central part of the as-grown crystal has been cut into individual samples for resistive and magnetization measurements. For the resistance measurements we have used a rectangular bar of size $6 \times 3 \times 1.6$ mm^3, with the longest dimension in $\langle 110 \rangle$ direction. Transport measurements were performed in a standard four-point arrangement with a separation between the voltage contacts of 0.3 mm. The dynamic resistance $R_d = dV/dI$ was measured using phase sensitive lock-in detection. An external magnetic field with a strength of up to 15 kOe could be applied in the direction parallel to the current flow (which was along the $\langle 110 \rangle$ crystalline direction). Volume magnetization measurements were performed by means of a vibrating sample magnetometer [17]. Transport and magnetization measurements were completed by magneto-optical imaging. A ferrimagnetic garnet indicator film with in-plane anisotropy was placed directly on top of the crystal and observed using linearly polarized light. The reflected light intensity, observed through an analyzer oriented nearly perpendicularly to the polarization direction, corresponds to the local value of the magnetic induction component perpendicular to the crystal and to the garnet.

Figure 1 shows the temperature evolution of the resistivity of the samples with $x = 0.22$ and $x = 0.18$ during thermal cycling in zero and non-zero applied magnetic field. Data obtained during zero field cooling (ZFC) down to 10 K, and subsequent heating to room temperatures are marked with open symbols. Observe that all ZFC heating and cooling lines fully overlap, there is no difference between an "up" and "down" temperature sweep. The data obtained during field cooling (FC) and subsequent heating in the same field of 14.5 kOe are shown with solid lines.

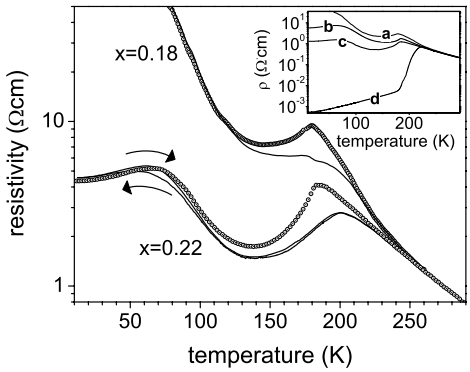

Fig. 1. Temperature dependence of the resistivity of $La_{0.78}Ca_{0.22}MnO_3$ and $La_{0.82}Ca_{0.18}MnO_3$ in zero magnetic field (open symbols) and at $H = 14.5$ kOe (solid line). Inset: Temperature dependence of resistivity of $La_{1-x}Ca_xMnO_3$ for various x: a) $x = 0.18$, b) $x = 0.2$, c) $x = 0.22$, d) $x = 0.3$.

The inset contains a set of ZFC characteristics recorded for various doping levels x. For all x the ZFC curves show a pronounced resistance maximum at a temperature T_p which is close to the relevant Curie temperature T_C determined from independent magnetization measurements. For example, for $x = 0.22$ we find $T_p \sim 186$ K and $T_C = 188 \pm 1$ K, see Figure 2. For underdoped crystals the resistivity at temperatures below T_p goes through a broad minimum, $T_{min} \sim 135$ K for $x = 0.22$, and turns up again to reach the second, low temperature maximum. Observe that even if the initial resistivity decrease, below T_C, has a metallic character with $\mathrm{d}\rho/dT > 0$, the resistivity values are much higher than those of optimally doped LCMO.

Application of a magnetic field significantly modifies the resistivity. The well known negative magnetoresistance (MR) effect is, as expected, most pronounced in the vicinity of the Curie temperature. FC curves for $x = 0.22$ show a pronounced thermal hysteresis at low temperatures. However, for very high, $T > 230$ K, and for very low, $T < 25$ K, temperatures the hysteretic effect is absent. Note that FC procedures bring about the positive MR effect during heating across the low temperature resistivity maximum. Due to the resistivity increase beyond the range of our measuring setup we cannot reveal whether the low temperature maximum exists for $x = 0.18$. We see only the beginning of the positive magnetoresistance effect at temperatures below 100 K.

Figure 2 shows the magnetic field dependence of the magnetization of LCMO single crystals with $x = 0.22$ and $x = 0.2$ at different temperatures below T_C. In a marked difference to the case with $x = 0.2$ (the magnetization for $x = 0.18$ is very close to that for $x = 0.2$ [17–19]) the

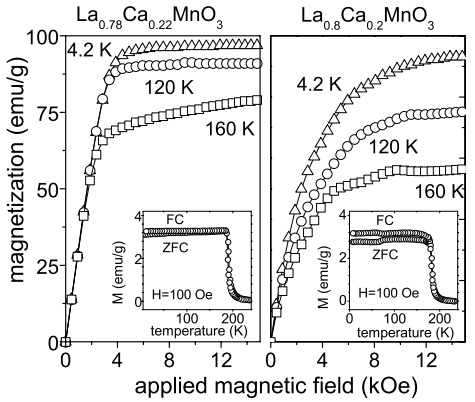

Fig. 2. Magnetization *vs.* magnetic field at various temperatures of 0.2 and 0.22 LCMO single crystals. Magnetic field is applied along the easy axis of (110) plane. Insets: Temperature dependence of the field cooled and zero field cooled magnetization as measured at 100 Oe.

field dependence of the magnetization of almost critically doped LCMO at $x = 0.22$ is very similar to that of an optimally doped LCMO at $x = 0.3$ and that of a conventional ferromagnet. With increasing field the initial almost linear increase of magnetization is followed by a saturation at fields above 3 kOe, whereas for lower doping levels the magnetization increases nonlinearly with field and does not fully saturate at 15 kOe, the maximum field available in our setup. Moreover, the temperature dependence of low field magnetization of critically doped LCMO shows no difference between ZFC and FC characteristics, while the difference is already clearly visible in the $x = 0.2$ case, see insets to Figure 2.

The dynamic resistance of optimally doped LCMO at $x = 0.3$ is practically current independent within the entire temperature and current range investigated. In a marked difference, the $I - V$ curves for $x = 0.18$, $x = 0.2$ and $x = 0.22$ are pronouncedly nonlinear. Since the current and field evolution of the $I - V$ characteristics of low doped LCMO with $x = 0.18$ have been published by us elsewhere [6,13,14], here we show only the current and field dependence for $x = 0.22$.

The current dependence of the dynamic resistance R_d at $H = 0$ and at $H = 14.5$ kOe is shown in Figure 3. At $T = 170$ K, just below the Curie temperature where the thermal coefficient of the resistivity is positive, $R_d(I)$ exhibits a broad maximum at zero bias. With increasing current the resistivity turns up and continuously increases. Application of a magnetic field moves the wide $R_d(I)$ minimum to higher currents, decreases the resistance and significantly reduces its sensitivity to the bias current. Close to the $R(T)$ minimum, at $T = 130$ K, $R_d(I)$ behavior becomes opposite to that at $T = 170$ K. The minimum at zero bias is accompanied by a broad maximum and a continuous decrease of the resistance with increasing current. The application of a magnetic field at 130 K influences only the resistivity value but does not change its sensitivity to the current flow. With further temperature decrease the general character of the $I - V$ curve does not change.

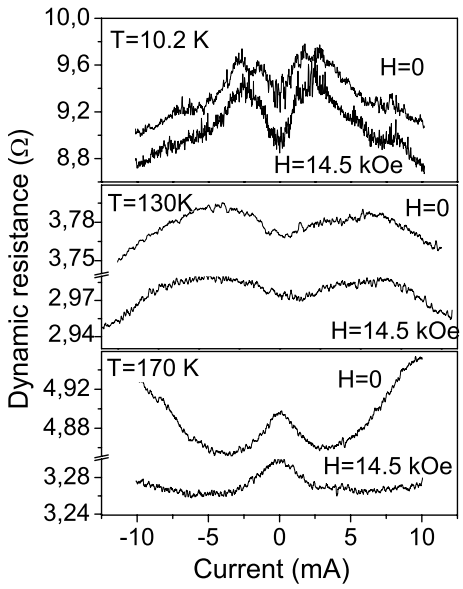

Fig. 3. Dynamic resistance (dV/dI) of $La_{0.78}Ca_{0.22}MnO_3$ single crystal *vs.* current at $H = 0$ and $H = 14.5$ kOe at 170 K, 130 K, and 10.2 K. Note the scale difference in 10.2 K graph.

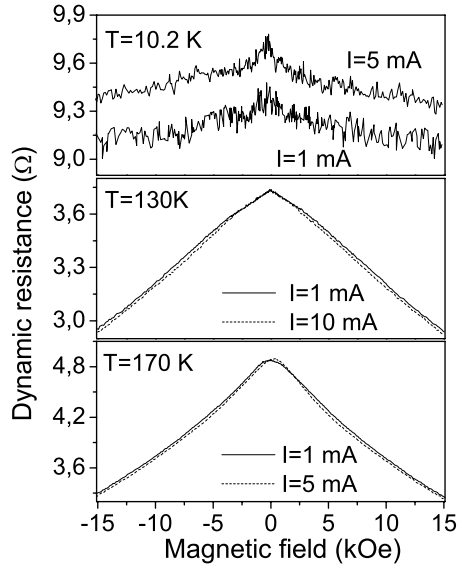

Fig. 4. Dynamic resistance of 0.22 LCMO crystal *vs.* magnetic field as seen at different bias currents and various temperatures.

However, at very low temperatures, below the second resistivity maximum, the bias current has a much stronger influence on the resistivity. At $T = 10.2$ K the resistivity variations observed in the entire ± 10 mA current range are close to 10%, while at higher temperatures they do not exceed 1%. Moreover, at low temperatures the maximum in $R_d(I)$ becomes more pronounced and moves to lower currents. On the other hand, at 10.2 K the MR effect is very small and the shape of the $R_d(I)$ characteristics does not change with field.

Figure 4 shows the R_d dependence on applied magnetic field at different currents and temperatures. At high temperatures the MR effect is so strong that it completely

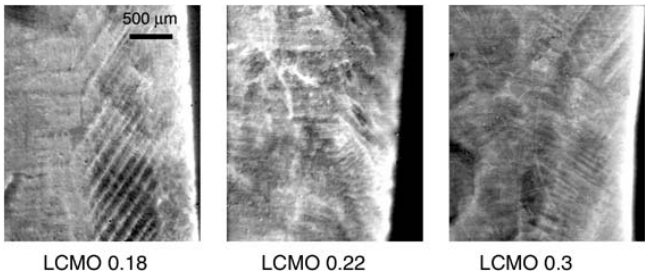

Fig. 5. Magneto-optical images of $La_{0.82}Ca_{0.18}MnO_3$, $La_{0.78}Ca_{0.22}MnO_3$, and $La_{0.7}Ca_{0.3}MnO_3$ single crystals in applied field of 250 Oe at $T = 25$ K. The $\langle 110 \rangle$ crystal axis lies in the plane of the micrograph and is directed along the longer edge of the picture. External magnetic field is applied perpendicular to the crystal surface. The dark areas on the right hand side of the micrographs lay beyond the crystal edge and indicate the strength of the applied field. The length of the dark bar in the upper right corner of the 0.18 LCMO image is 500 μm. The scale in the remaining images is the same.

masks any possible effect of current. At very low temperatures the MR effect is pronouncedly reduced and the current influence starts to be seen. The characteristics in Figure 4 were obtained in the ZFC regime. Observe that the sign of the MR effect for ZFC procedures is always negative in a difference to FC measurements illustrated in Figure 1. An interesting peculiarity is a clear suppression of resistivity fluctuations with increasing current at low temperatures.

Low-temperature magneto-optical images of 0.18, 0.22, and 0.3 LCMO crystals cooled in a uniform magnetic field perpendicular to the crystal plane are shown in Figure 5. The images represent the local field distribution on the plane containing the $\langle 110 \rangle$ axis. At high temperatures the crystals are paramagnetic and do not exhibit any magnetic contrast in their MO images. At $T < T_C$ the magnetic contrast structures in the form of parallel and almost periodic dark and bright stripes appears. The direction of the strip pattern coincides with the basic crystallographic directions. For example, the fish-bone quasi periodic strips in the 0.18 micrograph are directed along the $\langle 111 \rangle$ family (cubic structure). In the conditions of the experiment the higher value of the image intensity corresponds to the higher value of the local induction. We have verified that the local magnetic field is oriented in the same direction in the dark and in the bright regions. With decreasing temperature the aspect of the MO image does not change, one sees only an increase of the magnetic contrast with decreasing temperature and increasing field. Upon reversing the direction the applied field the high field areas again show a high intensity of the field but of opposite direction. The magnetic field in adjacent strips is oppositely oriented only when the external field is applied in the plane containing the $\langle 110 \rangle$ axis. Aside from the alternating orientation of the local induction, the shape and positions of the strip-like structures are identical for both perpendicular and in-plane direction of the applied field. The MO images obtained after turning off the field show remanent structures coinciding with those seen in applied field but the images obtained in ZFC regime practically do not show any magnetic contrast. The magnetic contrast does not represent therefore spontaneous ferromagnetic domains. The spontaneous magnetic domain structure, as it will be extensively discussed elsewhere, is significantly different from the magnetic contrast structures in MO images shown in Figure 5.

3 Discussion

The low temperature resistivity increase can be associated either with an increasing contribution of the orbitally ordered (OO) insulating ferromagnetic phase or with an increasing domination of the tunnel character of conductivity with decreasing temperature. Evidence for a tunnelling mechanism in $x = 0.18$ LCMO has been found through an excellent fit of the nonlinear $R_d(I)$ to the resonant indirect tunnelling models [6]. Current experiments with $x = 0.22$ crystals do not reveal any features characteristic for the tunnelling mechanism, such as a bell-shaped $R_d(I)$ characteristic or reproducible structures in the voltage dependence of the differential conductivity. Also, the nonlinear character of charge transport in $x = 0.18$ system is much more pronounced than in $x = 0.22$.

Magnetization jumps and frequency dependence of the susceptibility may be seen as a signature of the presence of OO phase in low doped 0.18 and 0.20 LCMO single crystals [17,18]. This is consistent with a pronounced difference between ZFC and FC magnetization, as shown in the insets to Figure 2. The positive MR effect showing out in a narrow temperature range in Figure 1 can also be seen as an indicator for the presence of the ferromagnetic insulating phase [20]. For the critically doped $x = 0.22$ LCMO we have not observed any magnetization jumps and almost no difference between the ZFC and FC low temperature magnetization. The temperature evolution of the ac susceptibility for $x = 0.2$ is similar to that for $x = 0.18$ but markedly different from that of $x = 0.22$; the susceptibility frequency dependence seen in $x = 0.22$ is much weaker than in sub-critically doped samples [17,18]. We conclude that the low temperature resistivity upturn in $x = 0.22$ LCMO is controlled by phase separation while in $x = 0.18$ tunnel mechanisms dominate, despite other indications suggesting that the presence of the orbitally ordered phase should be more pronounced in subcritically doped LCMO.

This discrepancy is consistent with the MO images. The magnetic contrast and strip-like structures are most pronounced in $x = 0.18$ LCMO. The contrast is weakest in the $x = 0.3$ MO image. The evolution of the MO images with changing direction of the applied magnetic field, the regularity of the pattern and the coincidence with the major crystallographic directions suggest that dark and bright strips represent twin domains. The magnetic contrast results from the crystalline magnetic anisotropy and represents how close the direction of the external magnetic field is with respect to the easy magnetization axis within the twin domain. We have previously associated

the intrinsic tunnel junctions in $x = 0.18$ LCMO with magnetic domain walls pinned by structural or growth defects [6,13,14]. The same defects give rise to the magnetic contrast in the MO images. The strength of the intrinsic tunnel barriers and their influence on the transport properties is proportional to the difference between the magnetization in adjacent domains, *i.e.*, to the MO image contrast [21,22].

The tunnelling mechanism can be also held responsible for the appearance of the second low temperature resistivity maximum. It has been demonstrated directly by introducing controlled artificial grain boundaries into epitaxial CMR films, that several in-series connected tunnel barriers along the current path cause strong nonlinearity of the $I-V$ curves accompanied by appearance of two maxima in the $R(T)$ dependence below T_C [21]. Remarkably, the interruption of the metallic percolation path with just one single barrier results only in an excess nonlinear resistivity, most pronounced at low temperatures, but not in the appearance of a second, low temperature, resistivity peak [22]. The average size of the twin domains in MO images is of the order of 100 μm. One may expect therefore that several tunnel barriers are incorporated between the voltage measuring contacts.

Finally we discuss strong resistivity fluctuations seen in the $R_d(I)$ dependence recorded at $T = 10.2$ K. The level of the resistivity noise increases by an order of magnitude with respect to that seen at 130 K or 170 K. A similar increase of the noise with decreasing temperature is not seen in Figure 1 because the $R_d(T)$ curves shown there have been measured using very large time constant of the lock-in amplifier which filtered out the fluctuations.

The most puzzling phenomenon is, however, the noise suppression by the current flow. In a classical situation of current independent resistivity fluctuations one should see a linear increase of the noise with increasing current. In our case the noise decreases with current indicating that the resistivity fluctuations are strongly current-dependent. However, in the $x = 0.22$ system we did not find any non-Gaussian fluctuations with current-dependent amplitude as is the case in $x = 0.18$ LCMO [14,15]. Non-Gaussian effects cannot account therefore for the exotic resistivity noise.

Spectral analysis has shown that the power spectra of $x = 0.22$ LCMO resistance noise are of the $1/f$ type. It is generally recognized that $1/f$-like spectra in solids originate from a superposition of many elementary two-level fluctuators (TLF) having a proper distribution of their characteristic cut-off frequencies. Each TLF is constituted by two energy wells separated by a barrier. TLF undergoes spontaneous transitions between the energy wells with a rate determined by the relative barrier height and generates elementary random telegraph waveform. Incoherent integration of the action of the entire ensemble of TLFs leads to $1/f$ spectrum. Each TLF generates a Lorentzian spectrum which, at frequencies below the cut-off frequency, is maximum when the transition probabilities between the TLF wells are identical. This happens in a symmetric TLF energy structure. With increasing asymmetry of the TLF one of the rates increases while the second one decreases. The characteristic Lorentzian cut-off frequency increases but the spectral density at low frequencies decreases progressively with increasing asymmetry of the fluctuator.

The exotic behavior of the low frequency noise in our crystal can be ascribed to a current dependence of the TLF energy structure. Assuming that all TLF in their pristine state, *i.e.*, at zero current flow, are symmetric, the decrease of the total noise with increasing current can be ascribed to the current enforced asymmetry of the TLF. The current induced force stressing the fluctuator energy structure can be either of the magnetic or of the electric origin. The relative insensitivity of the total noise to the applied magnetic field suggests that the interactions have most likely the electric nature.

In summary, we have investigated magnetic and transport properties of $La_{1-x}Ca_xMnO_3$ single crystals in the doping range $0.18 < x < 0.3$. The experiments involving measurements of electrical resistance, magnetoresistance, magnetization, and magneto-optics have revealed that crystals with Ca-doping level $x = 0.22$ close to the percolation threshold $x_C = 0.225$ cannot be treated as a simple intermediate case between optimally and subcritically doped case. In particular, tunnel conduction mechanism dominating in $x = 0.18$ LCMO is irrelevant for the critically doped crystal where the phase separation effects dominate, despite expectations that phase separation in $x = 0.18$ LCMO should be more pronounced than in critically doped $x = 0.22$ compound. Our results show that despite further evidence for existence of a mixed-phase ground state in low-doped CMR manganites the magneto-transport properties are also strongly influenced by the microcrystalline structure and the degree of twinning.

We thank D. Mogylanskii for X-ray characterization of our single crystals. Assistance in magnetization measurements offered by I. Fita and R. Puzniak and stimulating discussions with H. Shaked are greatly appreciated. This research was supported by the Israeli Science Foundation administered by the Israel Academy of Sciences and Humanities (grant 209/01).

References

1. M. Ziese, Rep. Prog. Phys. **65**, 143 (2002)
2. J.M. de Teresa, A. Barthelemy, J.P. Contour, A. Fert, J. Magn. Magn. Mater. **211**, 160 (2000)
3. J.Z. Sun, Physica C **350**, 215 (2001)
4. Moon-Ho Jo, N.D. Mathur, M.G. Blamire, Appl. Phys. Lett. **80**, 2722 (2002)
5. N.A. Tulina, S.A. Zver'kov, Y.M. Mukovskii, D.A. Shulyatev, Europhys. Lett. **56**, 836 (2001)
6. Y. Yuzhelevski, V. Markovich, V. Dikovsky, E. Rozenberg, G. Gorodetsky, G. Jung, D.A. Shulyatev, Ya.M. Mukovskii, Phys. Rev. B **64**, 224428 (2001)
7. T. Okuda, Y. Tomioka, A. Asamitsu, Y. Tokura, Phys. Rev. B **61**, 8009 (2000)

8. G. Biotteau, M. Hennion, F. Moussa, J. Rodriguez-Carvajal, L. Pinsard, A. Revcolevschi, Y.M. Mukovskii, D. Shulyatev, Phys. Rev. B **64**, 104421 (2001)
9. *Colossal Magnetoresistive Oxides*, edited by Y. Tokura (Gordon and Beach Science Publishers, 2000)
10. E. Dagotto, T. Hotta, A. Moreo, Phys. Rep. **344**, 1 (2001)
11. G. Papavassiliou, M. Belesi, M. Fardis, C. Dimitropoulos, Phys. Rev. Lett. **87**, 177204 (2001)
12. M. Belesi, G. Papavassiliou, M. Fardis, M. Pissas, J.E. Wegrowe, C. Dimitropulos, J. Dolinsek, Phys. Rev. B **63**, 180406R (2001)
13. V. Dikovsky, Y. Yuzhelevski, V. Markovich, G. Gorodetsky, G. Jung, D.A. Shulyatev, Ya.M. Mukovskii, Phys. Rev. B **65**, 144439 (2002)
14. Y. Yuzhelevski, V. Markovich, E. Rozenberg, G. Gorodetsky, G. Jung, D.A. Shulyatev, Ya.M. Mukovskii, J. Appl. Phys. **91**, 7397 (2002)
15. Y. Yuzhelevski, V. Dikovsky, V. Markovich, G. Gorodetsky, G. Jung, D.A. Shulyatev, Ya.M. Mukovskii, Fluct. Noise Lett. **1**, L105 (2001)
16. D.A. Shulyatev, A.A. Arsenov, S.G. Karabashev, Ya.M. Mukovskii, J. Cryst. Growth **198/199**, 511 (1999)
17. V. Markovich, I. Fita, R. Puzniak, M.I. Tsindlekht, A. Wisniewski, G. Gorodetsky, Phys. Rev. B **66**, 094409 (2002)
18. V. Markovich, E. Rozenberg, A.I. Shames, G. Gorodetsky, I. Fita, K. Suzuki, R. Puzniak, D.A. Shulyatev, Ya.M. Mukovskii, Phys. Rev. B **65**, 144402 (2002)
19. C.S. Hong, W.S. Kim, N.H. Hur, Phys. Rev. B **63**, 092504 (2001)
20. R. Senis, V. Laukhin, B. Martinez, J. Fontcuberta, X. Obradors, A.A. Arsenov, Y.M. Mukovskii, Phys. Rev. B **57**, 14680 (1998)
21. R. Gross, L. Alff, B. Büchner, B.H. Freitag, C. Höfner, J. Klein, Ya Feng Lu, W. Mader, J.B. Philipp, M.R.S. Rao, P. Reutler, S. Ritter, S. Thienhaus, S. Uhlenbruck, B. Wiedenhorst, J. Magn. Magn. Mater. **211**, 150 (2000)
22. C. Höfner, J.B. Philipp, J. Klein, L. Alff, A. Marx, B. Büchner, R. Gross, Europhys. Lett. **50**, 681 (2000)